An APPSO-SVM approach building the monitoring model of dam safety

Zhiping WEN
Nanjing Institute of Technology
Zhendong FAN
Hohai University
Huaizhi SU (su_huaizhi@hhu.edu.cn)
Hohai University https://orcid.org/0000-0001-6633-7851

Research Article

Keywords: dam safety, monitoring model, support vector machine, particle swarm optimization

Posted Date: April 14th, 2022

DOI: https://doi.org/10.21203/rs.3.rs-1536924/v1

An APPSO-SVM approach building the monitoring model of dam safety

Zhiping Wen[1], Zhendong Fan[2,3], Huaizhi Su[2,3,*]

Abstract

The measured data-based dam monitoring model could be used to analyze and predict the dam's operational behavior providing a scientific basis for risk assessment and decision-making of dam management. The traditional dam safety monitoring models established by multiple regression, stepwise regression, time series, gray theory, and other statistical methods have poor robustness and generalization. For this reason, an optimized support vector machine (SVM) whose novelty lies in simple execution procedure, self-adaptive hyperparameter selection from adaptive position particle swarm optimization (APPSO), user-friendly implementation and retention of influence factor combination, is presented for constructing the dam safety monitoring model.

Key words: dam safety; monitoring model; support vector machine; particle swarm optimization

1. Introduction

The historical measured data-based analysis and prediction for the dam's operational behavior has always been an important task during dam safety assessment. The measured data of dam monitoring projects, such as deformation, seepage, and stress-strain, could objectively reflect the health status of the dam such that it provides the scientific basis of dam safety monitoring model exerting the benefits of dam engineering under the premise of safe operation [1,2].

In recent years, there is a growing interest to find new alternatives of the traditional statistics-based dam monitoring models due to their limitations in low prediction accuracy, overfitting, poor generalization ability and so on [3]. Specifically, Chen established a chaotic dynamics-based dam monitoring model by calculating the Lyapunov exponent law reconstructed from monitoring data series [4]. In the works of Su et al., the support vector machine (SVM) was introduced to study the nonlinear and small sample problems of dam monitoring effects [5,6]; wavelet theory was applied to nonlinearly couple different dam monitoring sub-models [7,8]; chaos theory was used to identify the predictability of monitoring series [9]. Moreover, Ranković et al. presented a neural network-based dam monitoring model where the correlation and uncertainty of the influence factors are considered by fuzzy theory [10]. Furthermore, considering the sensitivity of the aforementioned machine learning methods to hyperparameter setting, the global optimization algorithms are adopted to optimize the hyperparameters for improving prediction accuracy of monitoring models. The cross-validation was employed to obtain the best parameters of SVM and neural network, respectively [11,12]; genetic algorithm was used for band selection [13,14]; particle swarm optimization algorithm was applied to optimized the

[1] Department of Computer Engineering, Nanjing Institute of Technology, Nanjing, China
[2] State Key Laboratory of Hydrology-Water Resources and Hydraulic Engineering, Hohai University, Nanjing, China
[3] College of Water Conservancy and Hydropower Engineering, Hohai University, Nanjing, China

Corresponding author:
Huaizhi Su, State Key Laboratory of Hydrology-Water Resources and Hydraulic Engineering, Hohai University, Nanjing 210098, China.
Email: su_huaizhi@hhu.edu.cn

hyperparameters of SVM [15,16]. However, it is worth noting that the implementation of aforementioned alternatives is cumbersome and expert-dependent that results in struggling application on practical engineering. Therefore, a modeling method with high fitting and predicting accuracy, strong generalization ability, and relatively simple structure is presented in this article.

In the proposed method, the SVM is introduced to process and construct the prototype observed data-based dam safety monitoring model due to its simple structure and powerful nonlinear fitting ability. Moreover, the adaptive position particle swarm optimization (APPSO) whose novelty lies in the enhanced searchability with the aid of inertia weight and learning factor, is adopted to optimize the penalty factor and kernel parameter of monitoring model.

2. SVM building the monitoring model of dam safety

The general principle of SVM is mapping the nonlinear variables of the input space to a linearly separable high-dimensional space with the aid of an inner product function (kernel function) and finally performing linear regression in the mapped space [16].

In the regression problem, assuming the training samples: (x_1,y_1), (x_2,y_2), …, $(x_i,y_i) \in (R^n \times R)$ and using a nonlinear mapping $\phi(\boldsymbol{x})$ to map the samples from the original space to a feature space with higher dimensions such that the optimal linear fitting function is built as the following form.

$$f(\boldsymbol{x}) = [\boldsymbol{\omega}, \boldsymbol{\phi}(\boldsymbol{x})] + b \tag{1}$$

where [•] denotes the inner product.

Next, optimizing the $\boldsymbol{\omega}$ and b for improving the generalization ability and controlling the complexity of the model. According to the principle of structural risk minimization, the optimization process could be equivalent to the following proposition:

$$\min \frac{1}{2}\|\boldsymbol{\omega}\|^2 + \frac{1}{2} C \sum_{i=1}^{l} \xi_i^2 \tag{2}$$

$$s.t. \quad y_i = \boldsymbol{\omega}^T \cdot \boldsymbol{\phi}(x_i) + b + \xi_i, \ i = 1,2,\mathrm{L}\ ,l \tag{3}$$

where $\boldsymbol{\omega}$ is weight factor; ξ_i is relaxation factor and $\xi_i \geqslant 0$; C is penalty factor and $C > 0$; b is a constant; l is the amount of training samples.

To solve the above optimization problem, the Lagrange function is introduced:

$$L(\boldsymbol{\omega}, b, \boldsymbol{\xi}, \boldsymbol{\alpha}) = \frac{1}{2}\|\boldsymbol{\omega}\|^2 + \frac{1}{2} C \sum_{i=1}^{l} \xi_i^2 + \sum_{i=1}^{l} \alpha_i \left[\boldsymbol{\omega}^T \cdot \boldsymbol{\phi}(x_i) + b + \xi_i - y_i \right] \tag{4}$$

where α_i is the multiplier of Lagrange function.

According to the condition of Karush-Kuhn-Tucker:

$$\frac{\partial L}{\partial \boldsymbol{\omega}} = 0, \frac{\partial L}{\partial b} = 0, \frac{\partial L}{\partial \boldsymbol{\xi}} = 0, \frac{\partial L}{\partial \boldsymbol{\alpha}} = 0 \tag{5}$$

Eq. (4) could be solved as the following form:

$$\begin{cases} \boldsymbol{\omega} = \sum_{i=1}^{i} \alpha_i \phi(x_i) \\ \sum_{i=1}^{i} \alpha_i = 0, \\ \alpha_i = C\xi_i \\ y_i - \boldsymbol{\omega}^T \cdot \phi(x_i) - b - \xi_i = 0 \end{cases} \tag{6}$$

Eliminating ξ_i and $\boldsymbol{\omega}$, the following linear equations are obtained:

$$\begin{bmatrix} 0 & \boldsymbol{e}^T \\ \boldsymbol{e} & K(\boldsymbol{x}, x_i) + \dfrac{\boldsymbol{I}}{C} \end{bmatrix} \begin{bmatrix} b \\ \boldsymbol{\alpha} \end{bmatrix} = \begin{bmatrix} 0 \\ \boldsymbol{y} \end{bmatrix} \tag{7}$$

where $\boldsymbol{e} = [1,1,\mathrm{L}\ ,1]^T$; $\boldsymbol{I}$ is the unit matrix of $l \times l$; $\boldsymbol{\alpha} = [\alpha_1, \alpha_2, \mathrm{L}\ , \alpha_l]^T$; $K(\boldsymbol{x}, x_i) = \phi(\boldsymbol{x}) \bullet \phi(x_i)$ denotes the inner product function, namely the kernel function.

As shown in Eq. (8), the radial basis kernel function (RBF) referred as the local sum function is employed in this article because of its high fitting precision.

$$K(\boldsymbol{x}, x_i) = \exp\left(-\frac{\|\boldsymbol{x} - x_i\|^2}{2\sigma^2} \right), \sigma > 0 \tag{8}$$

where σ is the Gaussian kernel parameter.

The final regression function of monitoring model is as follows:

$$f(\boldsymbol{x}) = \sum_{i=1}^{l} \alpha_i K(\boldsymbol{x}, x_i) + b \tag{9}$$

During constructing Eq. (9), penalty factor C balances the empirical risk and the structural risk, and kernel parameter σ determines the fineness of sample division. The larger C and smaller σ denote the curve is likely to be overfitting; reversely, the smaller C and larger σ represent the curve is likely to be underfitting. Therefore, the APPSO algorithm is introduced to optimize hyperparameter C and σ.

3. APPSO algorithm-based hyperparameter optimization of SVM

Particle Swarm Optimization (PSO) algorithm is inspired by bird foraging behavior and has been extensively applied on single-target and multi-target optimization issues due to its simple principle, easy implementation and high convergence velocity [17]. The standard PSO has the limitation in falling into local optimum, therefore the velocity factor and position factor are introduced to enhance the PSO's ability of jumping out the local optimum by judging the evolutional state of the population.

3.1. Standard PSO algorithm

In the PSO algorithm, each potential solution including the fitness and velocity of the optimization problem is called a particle. The fitness value used to indicate the superiority of particle is

determined by the fitness function. The velocity of particle determines the direction and step length of movement. The particles constantly update their position and velocity according to their cognition to themselves and group till finding the global optimal solution.

Specifically, in a *D*-dimensional searching space, the population $\boldsymbol{X} = \left(X_1, X_2, \mathrm{L}\ , X_n \right)^T$ is composed of *n* particles where the $\boldsymbol{X}_i = \left(X_{i1}, X_{i2}, \mathrm{L}\ , X_{iD} \right)^T$ and $\boldsymbol{V}_i = \left(V_{i1}, V_{i2}, \mathrm{L}\ , V_{iD} \right)^T$ are the position and velocity of the *i*-th particle, respectively; $\boldsymbol{P}_i = \left(P_{i1}, P_{i2}, \mathrm{L}\ P_{iD} \right)^T$ denotes individual extreme value p_{best}; $\boldsymbol{P}_g = \left(P_{g1}, P_{g2}, \mathrm{L}\ P_{gD} \right)^T$ represents the global extreme value of population g_{best}.

During each iteration, the particles update their position X_i and velocity V_i according to individual extreme value p_{best} and global extreme value g_{best}. The equations used for updating are described as follows:

$$V_{id}^{k+1} = \omega V_{id}^{k} + c_1 r_1 \left(P_{id}^{k} - X_{id}^{k} \right) + c_2 r_2 \left(P_{gd}^{k} - X_{id}^{k} \right) \tag{10}$$

$$X_{id}^{k+1} = X_{id}^{k} + V_{id}^{k+1} \tag{11}$$

where $d = 1, 2, \mathrm{L}\ D$, $i = 1, 2, \mathrm{L}\ n$; k is the current evolutionary algebra; ω is the inertia weight; c_1 and c_2 are the acceleration constants; r_1 and r_2 are the random numbers in $[0,1]$.

3.2. Improved PSO algorithm

In view of the limitation of standard PSO, an improved particle swarm optimization (APPSO) is presented.

The larger inertia weight ω represents stronger global searchability that the algorithm could search in a large range; the smaller ω denotes the stronger local searchability that the algorithm could perform fine search. At the beginning of iterations, algorithm should search in a large range for finding the global optimal solution and the higher search accuracy is needed in the later stages, therefore, the Linear Decreasing Weight (LDW) algorithm is proposed [18]. Its expression is as follows:

$$\omega = \omega_{\max} - i \times \left(\omega_{\max} - \omega_{\min} \right) \div j \tag{12}$$

where $\omega_{\max}$ and $\omega_{\max}$ are the maximum weight and minimum weight, respectively; *i* is the current evolutionary algebra; *j* is the maximum evolution algebra. In this article, the inertia weight decreases linearly from 0.9 to 0.3.

The factor c_1 denotes the influence weight of particle's own experience to its next behavior and the factor c_2 denotes the influence weight of other particles experiences to its next behavior.

During the optimization, factor c_1 linearly decreases and factor c_2 linearly increases [19].

$$c_1 = c_{1s} + i \times \left(c_{1e} - c_{1s} \right) \div j \tag{13}$$

$$c_2 = c_{2s} + i \times \left(c_{2e} - c_{2s} \right) \div j \tag{14}$$

where c_{1s}, c_{2s} are the initial iterative values of c_1, c_2, respectively; c_{1e}, c_{2e} are the final iterative values of c_1, c_2, respectively; i is the current evolution algebra; j is the maximum evolution algebra. In this article, the learning factor c_1 decreases linearly from 2.5 to 1 and factor c_2 increases linearly from 1.5 to 2.75.

It could be seen from Eq. (10) when the position of particle i is close to the global optimal value $\boldsymbol{P_g}$, its historical optimal value $\boldsymbol{P_i}$ is also close to $\boldsymbol{P_g}$; the latter two parts of the equation tend to zero; the velocity of particles does not substantially change. Similarly, the position of particles will also not change in Eq. (11). In view of the situation that the local optimum is regarded as the "global best" by the algorithm, the particle ‘s initialization criteria is presented as follows.

$$\begin{cases} d_{ij} = \left\| X_{ij} - P_{gj} \right\|_2 \\ d_{ij} < \gamma \\ V_{ij} < \upsilon \end{cases} \tag{15}$$

where υ is velocity factor; position factor $\gamma(\upsilon, \gamma \geq 0)$; $d_{ij} = \left\| X_{ij} - P_{gj} \right\|_2$ denotes the distance between the current position of the j-th dimension of the i-th particle and the global optimal position. When $d_{ij} < \gamma$ and the flying velocity $V_{ij} < \upsilon$, the particle is judged to be stagnant and the position of the particle is initialized before next iteration to prevent particle falling into local optimum.

4. Construction process of APPSO-SVM based dam monitoring model

Combined application of APPSO and SVM for constructing a dam safety monitoring model has the following specific steps and its flowchart is shown in Fig.1.

Step 1: Collecting the monitoring data of dam and its operational environment; selecting appropriate influence factors; dividing normalized sample data into training dataset and testing dataset.

Step 2: Applying the SVM to learn training dataset and obtaining the hyperparameters of SVM selected by APPSO.

Step 3: APPSO based hyperparameter optimization of SVM model.

(1) Initialization of population. Setting iteration number, population size, and optimization range of penalty factor C and kernel parameter σ; inertia factor ω adopts linear decreasing strategy; learning factor c_1 and c_2 adopt linear learning strategy; randomly setting the initial position x_i^0 and velocity v_i^0 of the particle in the optimization range.

(2) Fitness calculation. The accuracy rate of cross validation (CV) is individual fitness [20].

(3) Updating the velocity of particle according to Eq. (10); calculating distance d_{ij} and comparing d_{ij} with position factor γ; updating flight velocity V_{ij} and velocity factor υ. If $d_{ij} < \gamma$ and $V_{ij} < \upsilon$, reinitializing the position of particle, otherwise updating the position of particle according to Eq. (11).

(4) Comparing the fitness f_i of each particle with historical optimum p_{best}, only if $f_i < p_{best}$, $p_{best} = f_i$, otherwise f_i remains unchanged.

(5) Comparing the historical best fitness p_{best} of each particle with the optimal population value g_{best}, only if $p_{best} < g_{best}$, $g_{best} = p_{best}$, otherwise g_{best} remains unchanged.

(6) If the end condition is satisfied, the iteration is stopped, otherwise repeating (3)~(6).

Step 4: Verifying the SVM model. The obtained SVM model is tested with the testing dataset.

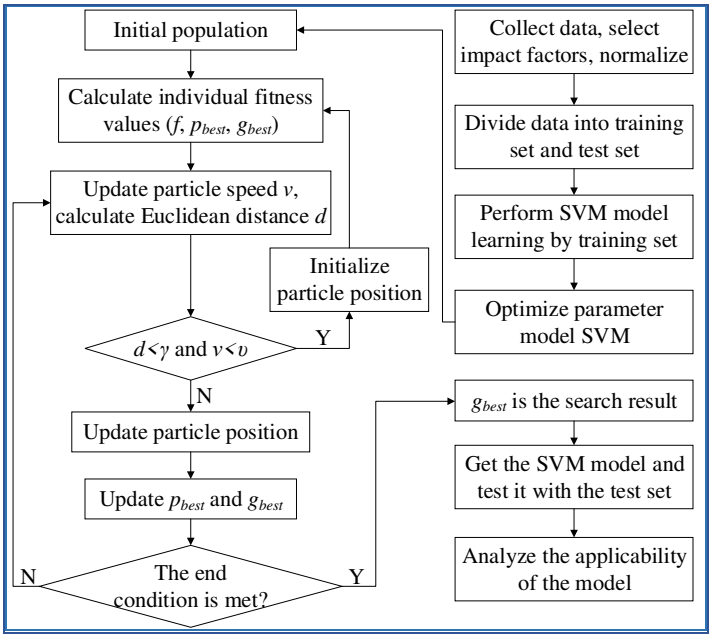

Fig.1. Construction flowchart of APPSO-SVM based monitoring model for dam safety.

5. Case Analysis

In this section, the presented method in this article is used to analyze the deformation behavior of a real-world gravity dam engineering and its performance is compared with classical benchmark methods.

5.1. Engineering and monitoring overview

A concrete gravity dam composed of 60 dam sections was built on the second main stream of Songhua River of China in 1937 and experienced renovation and expansion from 1951 to 1953.

The hub project consists of a concrete gravity dam, an overflow dam, a dam-behind hydropower plant, and a flood discharge tunnel. The maximum dam height is 91.7m, the length of dam crest is 1080m and the dam crest elevation is 267.70m. At present the total installed capacity of power generation is 1002.5MW and the average annual power generation is 19.68×10^{8}kW•h. The normal water level of the reservoir is 263.50m, the flood control water level is 260.50m, the dead water level is 242.00m, and the total storage capacity is 109.88×10^{8}m^{3}.

In order to ensure its safe operation, hundreds of measuring points are installed internal the dam to monitor horizontal deformation, vertical deformation, crack opening and uplift pressure. Over the past three decades, these points recorded nearly one million observations, where the deformation monitoring data is one of the most intuitive and comprehensive responses of dam behavior. Therefore, as shown in Fig.2, the horizontal dam crest deformation monitoring models of the 14#, 22# and 35# typical dam section, are analyzed and constructed by the proposed APPSO-SVM method.

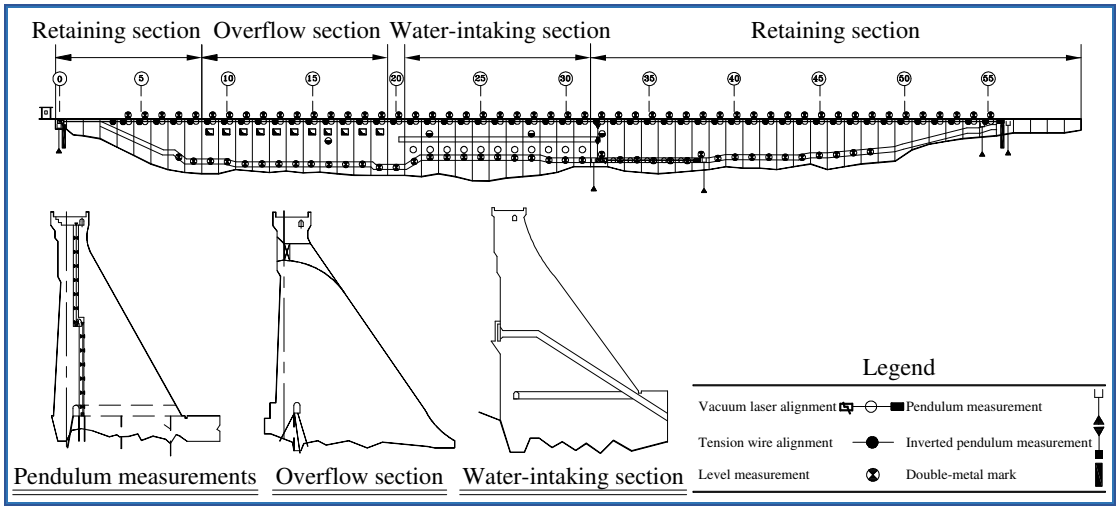

Fig.2. Layout of monitoring points of dam deformation.

5.2. Initial analysis for measured data

The data from the environment surrounded dam includes upstream water level, downstream water level, air temperature. The environmental measured values are shown in Fig.3. The horizontal dam crests displacement of the 14#, 22# and 35# dam sections is shown in Fig. 4.

Fig.3 indicates the highest water level in the upstream generally occurs from May to September with more rainfall. While the rainfall from January to March and December is less, corresponding lower upstream water level. The variation of upstream water level is within 15m from 2000 to 2010. The downstream water level is stable at 192m and the average annual variation is 2.36m. The temperature shows obvious annual cyclical changes. The highest annual temperature occurs from June to August, and the lowest temperature occurs from December to February of the following year. The annual temperature variation ranges from -30°C to 30°C.

In Fig. 4, the sign specifies the deformation toward downstream is positive and the deformation toward upstream is negative. Fig. 4 indicates the horizontal dam crest displacement of three typical dam sections is similar, and the maximum upstream deformation occurs in the 14# dam section, and the downstream maximum deformation occurs in the 22# dam section.

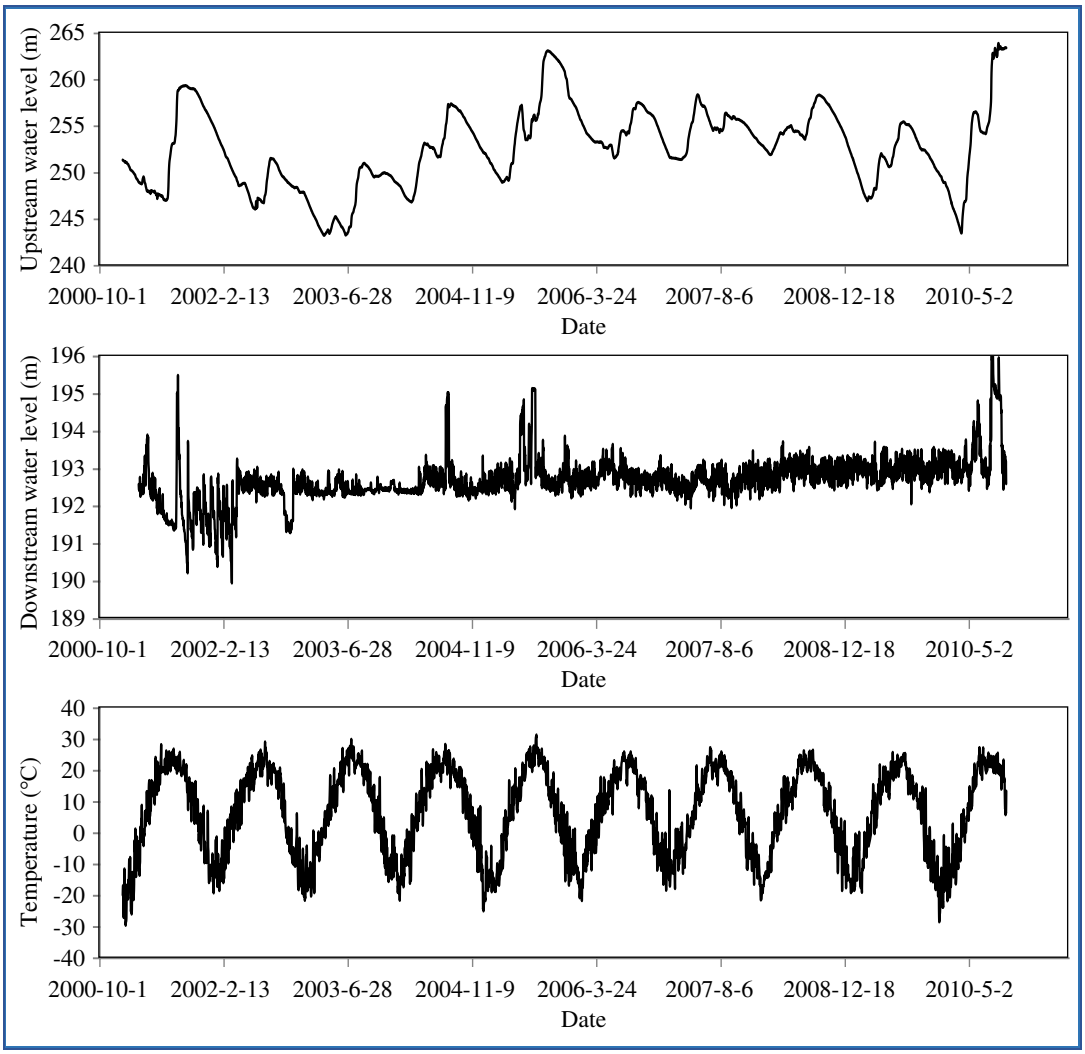

Fig.3. Time curve on observed environment.

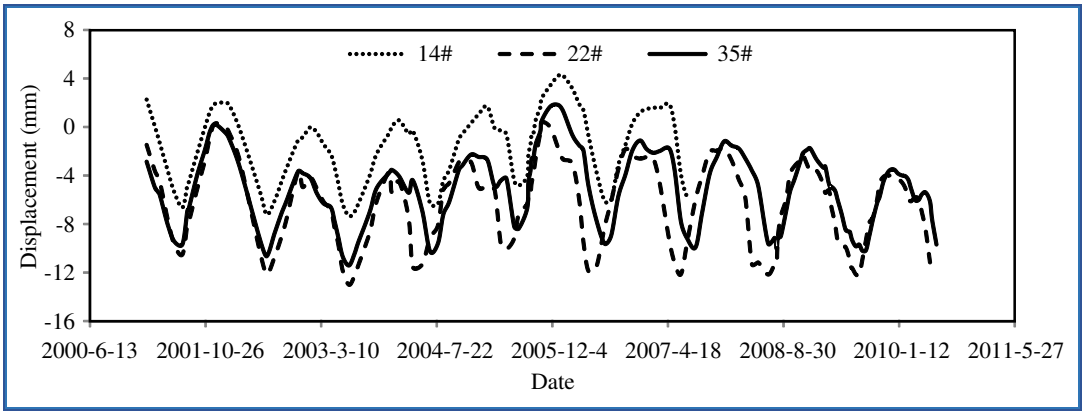

Fig.4. Time curve on observed horizontal radial displacement of three typical dam sections.

5.3. Monitoring model construction of dam deformation safety

The dataset is composed of upstream water level, downstream water level, air temperature, and the recorded horizontal displacement of dam crest in the 14#, 22# and 35# dam sections. Specifically, the training dataset is built by the data over a period from January 2001 to March 2010 and the testing dataset is from April 2001 to June 2010. The inputs of dataset are expressed as the

following form, and the outputs are composed of the horizontal displacement of analyzed dam section shown in Fig.4.

Water level component:

$$\left[H-H_0, H^2-H_0^2, H^3-H_0^3\right]$$

Temperature component:

$$\left[\sin\frac{2\pi it}{365}-\sin\frac{2\pi it_0}{365}, \cos\frac{2\pi it}{365}-\cos\frac{2\pi it_0}{365}, \sin\frac{4\pi it}{365}-\sin\frac{4\pi it_0}{365}, \cos\frac{4\pi it}{365}-\cos\frac{4\pi it_0}{365}\right]$$

Aging component:

$$\left[\theta-\theta_0, \ln\theta-\ln\theta_0\right]$$

where H is the current upstream water level; H_0 is the upstream water level at the beginning of observation; t denotes the cumulative days between the current observation date and the beginning observation date; t_0 represents the cumulative days between the starting observation date and the beginning date of the selected monitoring series; $\theta = t/100$ and $\theta_0 = t_0/100$.

After selecting the influence factors, the influence factors and the displacement effects are normalized in order to eliminate the influence of dimension between inputs and outputs. Assuming $X_{\max}$ and $X_{\min}$ are the maximum and minimum values of each group in sample data, then the corresponding standardized variables are as follows:

$$X' = 0.1 + 0.8\left(X - X_{\min}\right)/\left(X_{\max} - X_{\min}\right) \tag{16}$$

For evaluating performance of APPSO-SVM model, the statistical HST model, back propagation neural network (BPNN), and random forest regression (RFR) are selected as the benchmark monitoring models.

The parameters of APPSO-SVM are set as follows: the maximum iteration is 100; the population size is 30; the optimization range of penalty factor and kernel parameter are [0.05,5] and [0.001,0.1], respectively. Moreover, in the BPNN, the number of input layer equipped with hyperbolic tangent sigmoid function is 9 and the number of hidden layers equipped with linear function is 10; in the RFR, the number of leaves and trees are 30 and 200, respectively. The SVM hyperparameters of three typical dam sections optimized by APPSO are listed in Table 1.

Table 1. APPSO-SVM model hyperparameter.

Parameter	Hyperparameter value		
	14#	22#	35#
C	4.537	1.785	2.312
σ	0.940	0.441	0.577

The fitting curves of horizontal displacement are shown in Fig. 5 where the APPSO-SVM model generally outperforms other three benchmark models in terms of fitting deformation trend, peak displacement, trough position, and turning point.

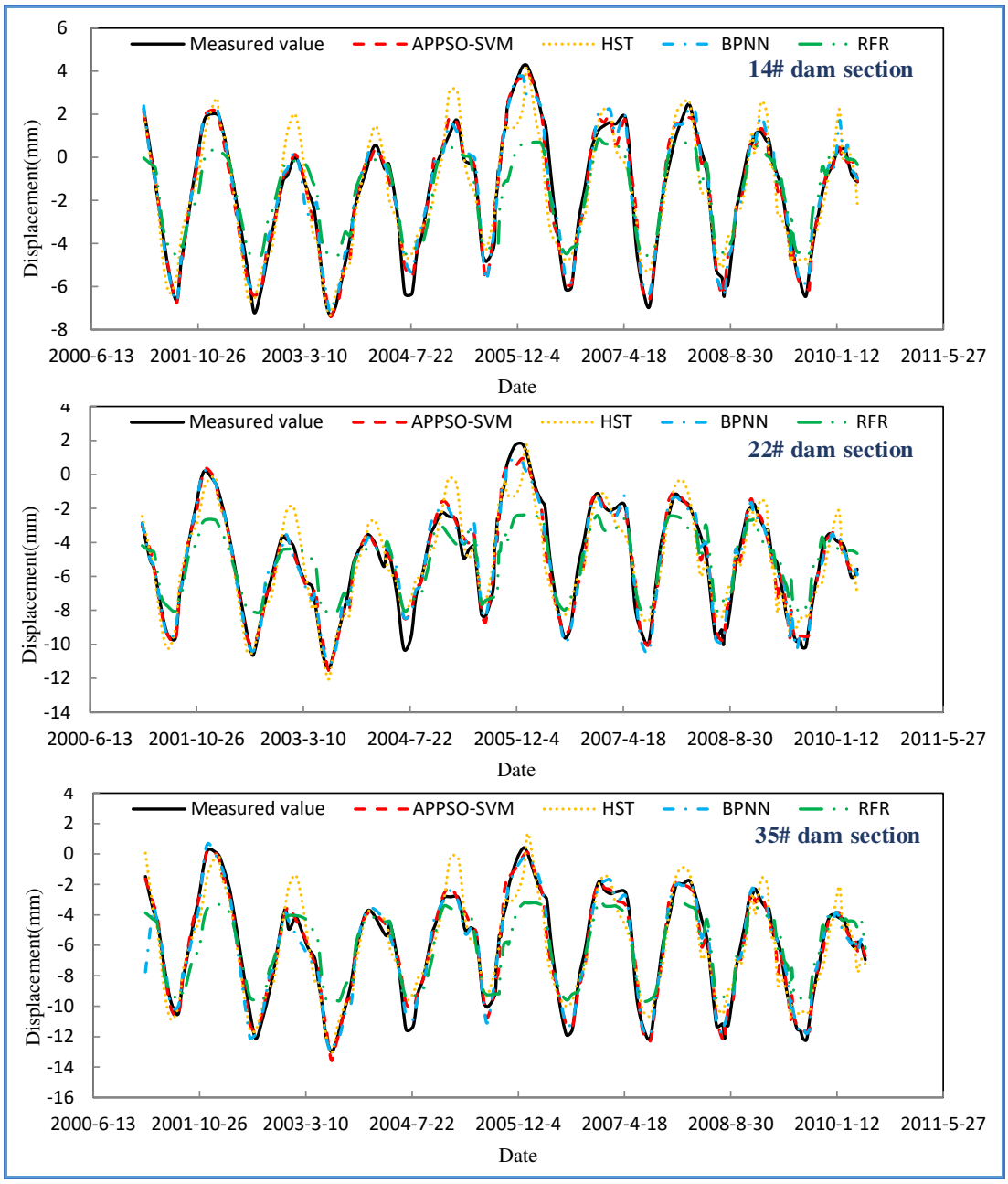

Fig.5. Calculated results of APPSO-SVM model and statistical model for three dam sections.

The fitting accuracy of APPSO-SVM model, statistical HST model, machine learning-based BPNN model and RFR model are shown in Table 2 and the corresponding computational time is listed in Table 3. The multiple correlation coefficients (R^2) of three displacement curves fitted by APPSO-SVM and BPNN are above 0.95 higher than HST model and RFR model, moreover, the computational modeling time of APPSO-SVM is less than BPNN indicating the proposed method has relatively strong generalization ability. From the perspective of mean square error (MSE) of training sample, the fitting ability of APPSO-SVM is better than benchmark models. On the other hand, the MSE of testing sample and the prediction error shown in Fig. 6 indicate the APPSO-SVM model has potential prediction ability outperforming benchmark models.

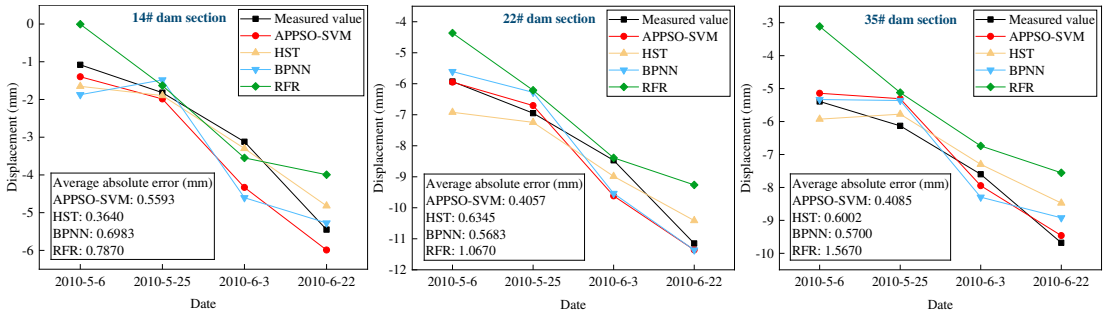

Fig.6. Predicted results of APPSO-SVM model and statistical model for three dam sections.

Table 2. Regression precision of APPSO-SVM and benchmark models for three dam sections.

Precision index	APPSO-SVM			HST			BPNN			RFR		
	14#	22#	35#	14#	22#	35#	14#	22#	35#	14#	22#	35#
R^2	0.977	0.979	0.970	0.930	0.934	0.929	0.965	0.970	0.967	0.662	0.674	0.599
MSE of training	0.472	0.642	0.614	1.051	1.238	1.142	0.525	0.778	0.585	1.375	1.653	1.624
MSE of testing	0.708	0.547	0.439	0.436	0.685	0.700	0.863	0.659	0.643	0.935	1.280	0.692

Table 3. Computational time of SVM-APPSO and benchmark models.

Dam section	Computational time (s)			
	APPSO-SVM	HST	BPNN	RFR
14#	0.2351	0.1062	0.3405	0.9385
22#	0.3795	0.1150	0.9378	1.0062
35#	0.2946	0.1492	0.7863	1.0545

6. Conclusions

The prototype dam data-based analysis and evaluation is an important part of dam safety monitoring playing an important role in properly identifying the operational risk. A novel support vector machine equipped with hyperparameter optimization from adaptive position particle swarm algorithm, simple execution procedure, and retention of influence factor combination is presented in this particle for monitoring model of dam safety.

a) Presenting a dam safety monitoring model based on the advantage of SVM in solving nonlinear, small sample, and high-dimensional regression problems. And penal factor and kernel parameter of the built monitoring model are optimized by an improved particle swarm algorithm whose novelty lies in the enhanced ability of avoiding local optimum.

b) The presented method is applied to modeling on horizontal dam crest displacement of a real-world concrete gravity dam engineering. The comparison with classical methods shows that the proposed method outperforms other benchmark method in terms of fitting and prediction accuracy.

Funding: This research has been partially supported by National Natural Science Foundation of China (SN: 51979093, 51739003), the National Key Research and Development Program of China (SN: 2019YFC1510801, 2018YFC0407101), Open Foundation of State Key Laboratory of Hydrology-Water Resources and Hydraulic Engineering (SN: 520003812), the Fundamental Research Funds for the Central Universities (Grant No. 2015B25414).

Conflict of Interest: The authors declare that they have no conflict of interest. Research do not involve human participants and/or animals.

References

1. Cheng L, Zheng DJ. Two online dam safety monitoring models based on the process of extracting environmental effect. Advances in Engineering Software, 2013, 57(1): 48-56.
2. Su HZ, Ren J, Wen ZP. An approach using Dempster-Shafer evidence theory to fuse multi-source observations for dam safety estimation. Soft Computing, 2019, 23(14): 5633-5644.
3. Salazar F, Moran R, Toledo MÁ, et al. Data-based models for the prediction of dam behavior: A review and some methodological considerations. Archives of computational methods in engineering, 2017, 24 (1): 1-21.
4. Chen J. Short-term prediction of observation data based on Lyapunov exponent. Journal of Hydraulic Engineering, 2001, 32(9): 64-67.
5. Su HZ, Chen ZX, Wen ZP. Performance improvement method of support vector machine-based model monitoring dam safety. Structural Control and Health Monitoring, 2016, 23(2): 252-266.
6. Su HZ, Li X, Yang BB, et al. Wavelet support vector machine-based prediction model of dam deformation. Mechanical Systems and Signal Processing, 2018, 110: 412-427.
7. Su HZ, Wu ZR, Wen ZP. Identification model for dam behavior based on wavelet network. Computer-Aided Civil and Infrastructure Engineering, 2007, 22(6): 438-448.
8. Su HZ, Chen J, Wen ZP, et al. Wavelet-fractal diagnosis model and its criterion for concrete dam crack status. Transactions of the Institute of Measurement and Control, 2018, 40(6): 1846-1853.
9. Su HZ, Wen ZP, Chen ZX, et al. Dam safety prediction model considering chaotic characteristics in prototype monitoring data series. Structural health monitoring, 2016, 15(6): 639-649.
10. Ranković V, Grujović N, Divac D, et al. Modelling of dam behaviour based on neuro-fuzzy identification. Engineering Structures, 2012, 35: 107-113.
11. Salazar F, Toledo MA, Oñate E, et al. An empirical comparison of machine learning techniques for dam behavior modeling. Structural Safety, 2015, 56: 9-17.
12. Mata J. Interpretation of concrete dam behaviour with artificial neural network and multiple linear regression models. Engineering Structures, 2011, 33(3): 903-910.
13. Xu C, Yue D, Deng C. Hybrid GA/SIMPLS as alternative regression model in dam deformation analysis. Engineering Applications of Artificial Intelligence, 2011, 25(3): 468-75.
14. Stojanovic B, Milivojevic M, Ivanovic M, et al. Adaptive system for dam behavior modeling based on linear regression and genetic algorithms. Advances in Engineering Software, 2013, 65: 182-190.
15. Su H, Li X, Yang B, et al. Wavelet support vector machine-based prediction model of dam deformation. Mechanical Systems and Signal Processing, 2018, 110: 412-427.
16. Su HZ, Wen ZP, Sun XR, et al. Rough set-support vector machine-based real-time monitoring model of safety status during dangerous dam reinforcement. International Journal of Damage Mechanics, 2017, 26(4): 501-522.
17. Yang LF, Su HZ, Wen ZP. Improved PLS and PSO methods-based back analysis for elastic modulus of dam. Advances in Engineering Software, 2019, 131: 205-216.
18. Liu HW, Lin YX, Qi MJ, et al. Improved particle swarm optimization algorithm for solving constrained optimization problems. Journal of Northeast Petroleum University, 2005, 29(4): 73-75.
19. Asanga R, Saman KH, Harry CW. Self-organizing hierarchical particle swarm optimizer with time-varying acceleration coefficients. IEEE Transactions on Evolutionary Computation, 2004, 8(3): 240-255.
20. Oh HS, Kim D, Lee, Y. Cross-validated wavelet shrinkage. Computational statistics, 2009, 24(3): 497-512.